Photonic bands, gap maps, and intrinsic losses in three-component 2D photonic crystal slabs

Hongjun Shen (沈虹君)[1,2*], Huiping Tian (田慧平)[1], and Yuefeng Ji (纪越峰)[1]

[1] *Key Laboratory of Optical Communication and Lightwave Technologies, Ministry of Education, School of Telecommunication Engineering, Beijing University of Posts and Telecommunications, Beijing 100876*

[2] *School of Physics and Electrical Information Science of Ningxia University, Yinchuan 750021*

[*] *E-mail: shenhongj2004@126.com*

Received June 23, 2008

We obtain the photonic bands and intrinsic losses for the triangular lattice three-component two-dimensional (2D) photonic crystal (PhC) slabs by expanding the electromagnetic field on the basis of waveguide modes of an effective homogeneous waveguide. The introduction of the third component into the 2D PhC slabs influences the photonic band structure and the intrinsic losses of the system. We examine the dependences of the band gap width and gap edge position on the interlayer dielectric constant and interlayer thickness. It is found that the gap edges shift to lower frequencies and the intrinsic losses of each band decrease with the increasing interlayer thickness or dielectric constant. During the design of the real PhC system, the effect of unintentional native oxide surface layer on the optical properties of 2D PhC slabs has to be taken into consideration. At the same time, intentional oxidization of macroporous PhC structure can be utilized to optimize the design.

OCIS codes: 160.0160, 300.0300, 300.6170..

doi: 10.3788/COL20090703.0231.

Development of ultrasmall optical integrated circuits using two-dimensional (2D) photonic crystal (PhC) slab is currently the subject of intense investigation[1−6]. The initial stage for the formulation of numerical proposals on a wide variety of PhC structures, such as straight, sharp-bend, and junction structures has been followed by the second stage for practical demonstrations in real optical systems. For example, several research groups have demonstrated the disorder-induced loss[7,8], sidewall roughness-induced loss[9], and radiation losses in the case of finite hole depth and cylindroconical hole shape[10]. All the works concern the problem of fabrication imperfections in PhCs. It is not surprising that the imperfection disorders in PhCs are focused on, because they are inevitable in fabrication. In addition to fabrication imperfection, another inevitable problem is oxidization of PhC slabs in air. If a device does not work in vacuum, the PhC's "atoms" may slightly change their properties near the interfaces due to some chemical processes. The inner pore's surface of a macroporous slab structure inevitably contains oxide interlayer which has the properties different from the bulk ones. Up to date, little work has been done about this problem except the work of Glushko *et al.*[11]. However, the structure they dealt with was ideal 2D PhC which was actually unsuitable for practical applications. On the contrary, 2D PhC slabs can provide sufficient confinement in the vertical direction because of the index differences, and what is more, the fabrication of 2D PhC slabs is compatible with modern planar semiconductor processing technology, making them promising for highly dense photonic integrated circuits. In order to understand the optical properties of 2D PhC slabs enough, it is therefore necessary to investigate the dependences of the properties of PhC slabs on various structure parameters including the parameters of oxide surface layer.

Furthermore, the intentional interlayer of the macroporous structure is widely used[12−15]. For PhC slabs, the introduction of extra component enlarges our freedom for fine-tuning the dispersion properties. As a matter of fact, the fabrication of PhC slab which allows to tune the photonic band gap edges by an external influence has been one of the recent investigation directions. There are many mature technologies which can be used to introduce interlayer into macroporous PhC slabs, for example, thermal oxidation, oxide etching, and atomic layer deposition (ALD)[16]. Among them, ALD is more promising because it enables a high degree of control over material and structural properties, which allows for precise static tuning of optical properties. With ALD, films can be grown on the inner pore's surface of a macroporous slab with a precision of 0.05 nm[15].

In this letter, we investigate theoretically the three-component 2D PhC slab for which the 2D PhCs are embedded in a planar waveguide and the third medium with thickness d is introduced as a ring-shaped intermediate layer around the hole's surface, as shown in Fig. 1. The slab of thickness h with triangular array of air holes of radius R is suspended in air. The dielectric constants of the background medium, inside air holes, and intermediate layer are denoted as $\varepsilon_{\rm b}$, $\varepsilon_{\rm a}$, and $\varepsilon_{\rm i}$, respectively. This structure is referred to as an air bridge. We define the lattice constant as a. The light propagating in the horizontal direction is dominated by the photonic band gap (PBG) and the total internal reflection confines the light in the vertical direction. In order to provide low optical radiation loss in PhC slab, a core/clad structure with a high refractive-index contrast in the vertical direction is a virtual requirement for strong vertical confinement. So silicon is often chosen as the core layer due to its high dielectric constant ($\varepsilon = 11.7$) and the sophisticated technique for Si slab nanofabrication.

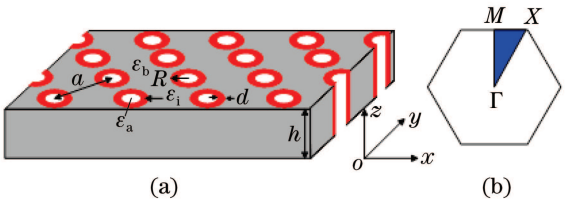

Fig. 1. Schematic structure of triangular lattice of circular air holes with intermediate layer in a PhC slab. (a) Slab waveguide of thickness h patterned with a triangular lattice of circular air holes with intermediate layer; (b) 2D Brillouin zone and symmetry points.

For a periodic dielectric constant $\varepsilon(\vec{r})$, a Bloch state for the magnetic field at the nth band and wave vector $\vec{k}$ satisfies the Maxwell equation

$$c^2\nabla\times[\varepsilon^{-1}(\vec{r})\nabla\times H_{nk}(\vec{r})]=\omega_{nk}^2 H_{nk}(\vec{r}), \tag{1}$$

where ω_{nk} and $H_{nk}(\vec{r})$ are the eigenfrequencies and eigenvectors, respectively. After the insertion of a third component, the new dielectric function, eigenfrequencies, and eigenvectors are denoted as $\tilde{\varepsilon}(\vec{r})$, $\tilde{\omega}_{nk}$, and $\tilde{H}_{nk}(\vec{r})$. Ignoring the higher order terms, from perturbation theory, it is easy to obtain from Eq. (1) that

$$\begin{aligned}&\nabla\times\varepsilon^{-1}(\vec{r})\nabla\times\delta H_{nk}\\&+\nabla\times[\tilde{\varepsilon}^{-1}(\vec{r})-\varepsilon^{-1}(\vec{r})]\nabla\times H_{nk}(\vec{r})\\&\cong\frac{\tilde{\omega}_{nk}^2-\omega_{nk}^2}{c^2}H_{nk}+\frac{\omega_{nk}^2}{c^2}\delta H_{nk},\end{aligned} \tag{2}$$

where $\tilde{H}_{nk}=H_{nk}+\delta H_{nk}$. By some mathematical strategies[12], we finally obtain

$$\left(\frac{\tilde{\omega}_{nk}}{\omega_{nk}}\right)^2-1\approx\frac{\int[\tilde{\varepsilon}^{-1}(\vec{r})-\varepsilon^{-1}(\vec{r})]\,|D_{nk}(\vec{r})|^2\,\mathrm{d}r}{\int\varepsilon^{-1}(\vec{r})\,|D_{nk}(\vec{r})|^2\,\mathrm{d}r}, \tag{3}$$

where the integration is over a unit cell, $D_{nk}(\vec{r})$ is displacement field. $\tilde{\varepsilon}^{-1}(\vec{r})-\varepsilon^{-1}(\vec{r})$ is nonzero, say, δ, only at the insertion position. In our case, $\delta<0$, so from Eq. (3), it can be followed that $\tilde{\omega}_{nk}<\omega_{nk}$, which indicates that the bands shift downwards. What is more, according to the electromagnetic variational theorem[1], the low-frequency modes concentrate their energy in high ε regions and high-frequency modes concentrate their energy in low ε regions. The insertion of the third medium ($\varepsilon>1$) affects higher-frequency modes more strongly, which implies that the higher-frequency modes shift downwards larger than the lower-frequency modes do.

The perturbative approach above explains a physical origin of the shift of bands in PhC slabs with interlayers. However, owing to ignoring the higher-order terms, one can only obtain approximate results by Eq. (3)[15]. In this letter, we use the guided-mode expansion (GME) method to calculate more accurately the electromagnetic wave propagation through the 2D dielectric lossless PhC slabs. GME has already been described in detail before[17,18]. The basis of Fourier expansion we apply contains 259 vectors of reciprocal lattice and 4 guided modes of the effective waveguide, which is sufficient for convergence in calculation of photonic eigenmodes. So photonic eigenmodes obtained by the present approach can be considered reliable and accurate.

The 2D triangular lattice PhC slab that we are considering is depicted in Fig. 1. Compared with general air-clad waveguides, there are additional interlayers on the inner pore's surface. The waveguide is symmetric.

In the symmetric PhC slab, the waveguide modes can be classified into TE-like modes and TM-like modes. Only for the TE-like modes, there exits band gap, which is usually used in PhC devices. For the TM-like modes, there does not exist band gap in general. So in this work we only calculate the band gap of TE-like modes. Figure 2 shows the photonic mode dispersion for the lowest TE-like gap in the triangular lattice PhC slab with $R=0.45a$, $h=0.45a$. The photonic mode dispersion is represented in dimensionless units, $a/2\pi c$ for the frequency, and a/π for the wave vector. The shaded region represents the continuum of TE-like slab modes of the triangular lattice folded in the Brillouin zone. We can see from Fig. 2 that compared with the case of no interlayer, the bands of the PhC slab containing the additional interlayer ($\varepsilon_i>1$) shift downwards, which agrees well with the perturbative approach analysis above. In addition, it follows from electromagnetic variational theorem that the higher the band, the larger its frequency shift downwards, which results in a narrower band gap. All of these can be seen from Fig. 2.

We studied the dependence of the shifts of band edges on the thickness of the interlayer. Figure 3(a) shows the effect of interlayer of thickness d on the band edges of the

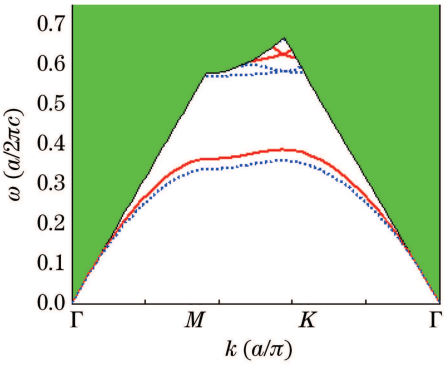

Fig. 2. Photonic bands of PhC slab of $R=0.45a$, $h=0.45a$, $\varepsilon_a=1$, $\varepsilon_b=12$. Dotted lines represent photonic bands with interlayer of thickness $d=0.02a$, $\varepsilon_i=10$. Solid lines represent the photonic bands without interlayer.

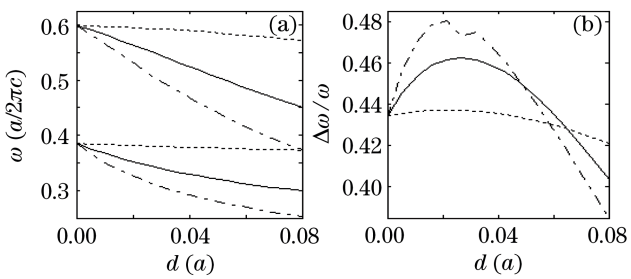

Fig. 3. (a) Band edges of the lowest gap as a function of interlayer thickness d. (b) Ratio of the gap width ($\Delta\omega$) to the mid-gap frequency (ω) as a function of d. Dotted lines correspond to $\varepsilon_i=2$, solid lines correspond to $\varepsilon_i=12$, dashed lines correspond to $\varepsilon_i=24$.

Table 1. Positions of TE-Like Mode Gap Edges for Different Interlayer Thicknesses, R=0.45a, ε_i= 4

d	2D Ideal PhC		PhC Slab with $h = 0.45a$		PhC Slab with $h = 0.3a$	
	λ_l (μm)	λ_u (μm)	λ_l (μm)	λ_u (μm)	λ_l (μm)	λ_u (μm)
0	1.670	1.025	1.293	0.8300	1.170	0.770
0.01a	1.704	1.036	1.314	0.8361	1.185	0.777
0.02a	1.729	1.049	1.332	0.8464	1.201	0.790

λ_l represents the gap edge of the lower mode, λ_u represents the gap edge of the upper mode.

lowest gap. From Eq. (3), it follows that the gaps edges shift to lower frequencies with the increase of thickness of silica interlayer on the surface of the pores. Furthermore, in the structure with larger interlayer dielectric constant, the shift of the band edges is larger. From Fig. 3, it is clear that even the interlayer of the thickness $d = 0.01a$ can influence the gap edge positions. We estimated quantitatively the shift of the gap edge positions for some real structures with constants $a = 0.5$ μm, radius $R = 0.225$ μm, and the interlayer thickness d changing from 0 to 40 nm. Table 1 shows the values of the TE-like gap edges of PhC slabs with three different thicknesses. In the PhC slab with the thickness of 0.45a, in comparison with the case of no interlayer, relative shifts of the band gap edges have the values of about 1.62% for the interlayer thickness $d = 0.01a$ and 3.02% for $d = 0.02a$, the absolute values of the shifts are over 20 nm. Shift of the gap edges in a 2D silicon PhC due to Kerr effect achieved in Ref. [19] was about 30 nm, which is of the same order with the shifts shown in Table 1. Thus, in some cases, especially for the structures with small lattice pitch ($a < 1$ μm), one has to take the effect of extra oxide layer into consideration for correction[11]. In addition, we investigated the effect of oxide interlayer in PhC slab of different thicknesses. In the case of $h = 0.3a$, relative shifts of the band gap edges are near 1.28% for the interlayer thickness $d = 0.01a$ and 2.65% for $d = 0.02a$ that are evidently less than those in PhC slab of $h = 0.45a$. The effect of oxide interlayer is sensitive to the slab thickness. The thicker the slab is, the more sensitive the effect of oxidized interlayer is.

Figure 3(b) shows the normalized width at the mid-gap as a function of the interlayer thickness d. The overall tendency is clearly seen: the normalized width first monotonously rises to a peak at certain d and then monotonously decreases with the increase of d. There is always a thickness range in which the normalized width is larger than that in the case of without interlayer. It is noted that at a relatively thicker interlayer (about $> 0.7a$), the larger ε_i is, the smaller the normalized width is. As a matter of fact, in the PhC slab with thickness 0.45a which does not contain oxide interlayer, the normalized width reaches its maximum at $R = 0.436a$. Due to the appearance of oxide interlayer, the radius of air holes in the PhC slab reduces, the normalized width increases, and the peak appears at different R around 0.436a, which depends on the interlayer dielectric constant. The less the dielectric constant of interlayer is, the bigger radius the peak appears at.

Next, we consider the dependence of the shifts of band edges on the dielectric constants of the interlayer. In Fig. 4(a), we present the gap map for the structure with

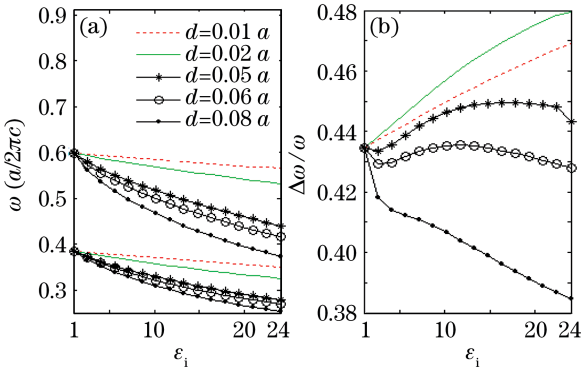

Fig. 4. (a) Band edges of the lowest gap as a function of dielectric constant ε_i of interlayer. (b) Ratio of the gap width $\Delta\omega$ to the mid-gap frequency ω as a function of ε_i.

different interlayer dielectric constants for PhC slabs with $R = 0.45a$, $h = 0.45a$, and different interlayer thicknesses of $d = 0.01a$, $0.02a$, $0.04a$, $0.06a$, $0.08a$. The increase of effective dielectric constant results in shifts of the gaps towards lower frequencies, and the thicker the interlayer is, the lower the band gap edge is. From Fig. 4(b), we can see that with ε_i growing, the normalized width grows at thin interlayer (about $< 0.07a$) and decreases at thick interlayer ($> 0.07a$). In fact, this agrees with Fig. 3(b).

In PhC slab systems, a few photonic modes lie below the light line of the cladding material and are truly guided, which should be lossless in an ideal PhC structure without imperfections. Whereas those modes lying above the light line are subject to intrinsic radiation losses due to the out-of-plane diffraction. The light line problem represents an intrinsic limit for the application of PC slabs to integrated photonics. It is therefore important to quantify the level of intrinsic losses and to know their dependence on the structure parameters. This is done by using time-dependent perturbation theory for the electromagnetic problem[16]. We calculated the intrinsic losses for several lowest photonic bands, part of which lie below the light line and can be used as lossless modes. The results are presented in Table 2 and Fig. 5. From Figs. 5(a) and (c), we can find that for a certain thick interlayer, the bands shift downwards with the growing dielectric constant. Figures 5(b) and (d) show the propagation losses of the second and third bands of PhC slab with various interlayer dielectric constants. With the red-shift of photonic bands, the bands cross the light line in air and become true guided mode, and at the crossing point frequency the radiation losses approach to zero. Owing to the insertion of interlayer, the frequency range of each mode, in which the mode is subject to intrinsic radiation losses, becomes narrower. The modes in this frequency range become flatter, which results in a lower group velocity. It is clear from Table 2 that the radiation losses generally decrease with the increasing interlayer dielectric constant. In addition, from Fig. 5(c) we can find that the third bands of PhC slabs with different interlayer dielectric constants, near the edge of Brillouin zone (Γ point), are very flat, which implies a low group velocity. It is well known that the propagation losses depend on the group velocity strongly and this explains the fact that in Fig. 5(d), near Γ point, the loss grows rapidly.

Table 2. Losses of the Lowest Two Bands for Different Interlayer Dielectric Constants

ε_i	The Second Band		The Third Band	
	ω_c $(a/2\pi c)$	L_M (dB/mm)	ω_c $(a/2\pi c)$	L_M (dB/mm)
1	0.5989	13.6	–	2.78
5.5	0.5499	5.156	0.6475	0.4104
10	0.5151	3.606	0.6193	0.0539
14.5	0.4859	3.123	0.6030	1.457×10^{-4}

ω_c is the frequency at the crossing point between photonic bands and air-cladding light line, L_M represents the maximum loss over the frequency range, in which modes are subject to intrinsic loss (except Γ point), that is, the frequency range between ω_c and the frequency at Γ point.

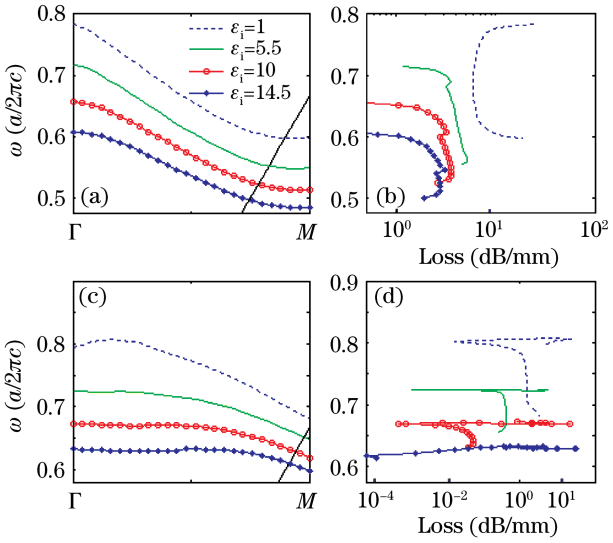

Fig. 5. Propagation losses for two photonic bands of PhC slabs with different dieletric constants of interlayer, $R = 0.45a$, $h = 0.5a$, $d = 0.04a$. (a) The second band for four different values of ε_i; (b) propagation losses corresponding to the second band; (c) the third band for four different values of ε_i; (d) propagation losses corresponding to the third band.

In summary, we have performed systematic studies on the influence of the pore surface interlayer on the optical properties of 2D PhC slabs. The insertion of even thin low-index interlayer significantly influences the TE-like gap edges. What is more, besides offering more chance to modify the dispersion properties of the PhC slab, the additional interlayer in PhC slabs have a positive impact on the losses.

This work was supported in part by the National Natural Science Foundation of China (No. 60707001, 60711140087), the National "973" Program of China (No. 2007CB310705), the National "863" Program of China (No. 2007AA01Z247), NCET (07-0110), PCSIRT (No. IRT0609), and ISTCP (No. 2006DFA11040), P. R. China.

References

1. J. D. Joannopoulos, R. D. Meade, and J. N. Winn, *Photonic Crystals: Molding the Flow of Light* (Princeton University Press, Princeton, 1995).
2. Y. Benachour and N. Paraire, Chin. Opt. Lett. **5,** 501 (2007).
3. Z. Zhou, X. Huang, R. Vanga, and R. Li, Chin. Opt. Lett. **5,** 693 (2007).
4. H. Wang, J. Wang, W. Li, and W. Ding, Chin. Opt. Lett. **6,** 431 (2008).
5. C. Tan, X. Huang, and G. Fan, Acta Opt. Sin. (in Chinese) **27,** 482 (2007).
6. Y. Li, P. Gu, B. Wang, Z. Zhen, and X. Liu, Acta Opt. Sin. (in Chinese) **28,** 169 (2008).
7. D. Gerace and L. C. Andreani, Opt. Lett. **29,** 1897 (2004).
8. R. Ferrini, D. Leuenberger, R. Houdré, H. Benisty, M. Kamp, and A. Forchel, Opt. Lett. **31,** 1426 (2006).
9. W. Bogaerts, P. Bienstman, and R. Baets, Opt. Lett. **28,** 689 (2003).
10. R. Ferrini, B. Lombardet, B. Wild, R. Houdré, and G.-H. Duan, Appl. Phys. Lett. **82,** 1009 (2003).
11. A. Glushko and L. Karachevtseva, Photon. Nanostruct. **4,** 141 (2006).
12. X. Zhang, Z.-Q. Zhang, L.-M. Li, C. Jin, D. Zhang, B. Man, and B. Cheng, Phys. Rev. B **61,** 1892 (2000).
13. X. Zhang and Z.-Q. Zhang, Phys. Rev. B **61,** 9847 (2000).
14. T. Trifonov, L. F. Marsal, A. Rodríguez, J. Pallarès, and R. Alcubilla, Phys. Rev. B **70,** 195108 (2004).
15. E. Graugnard, D. P. Gaillot, S. N. Dunham, C. W. Neff, T. Yamashita, and C. J. Summers, Appl. Phys. Lett. **89,** 181108 (2006).
16. M. Thitsa, Y. Song, and S. Albin, J. Electrochem. Soc. **155,** H351 (2008).
17. L. C. Andreani and D. Gerace, Phys. Rev. B **73,** 235114 (2006).
18. L. C. Andreani and M. Agio, IEEE J. Quantum Electron. **38,** 891 (2002).
19. H. W. Tan, H. M. van Driel, S. L. Schweizer, R. B. Wehrspohn, and U. Gösele, Phys. Rev. B **70,** 205110 (2004).